

Increasing-Margin Adversarial (IMA) Training to Improve Adversarial Robustness of Neural Networks

Linhai Ma & Liang Liang

Department of Computer Science, University of Miami
1365 Memorail Drive, Coral Gables, FL, USA
l.ma@miami.edu & liang@cs.miami.edu

Abstract

Convolutional neural networks (CNN) have surpassed traditional methods for medical image classification. However, CNNs are vulnerable to adversarial attacks which may lead to disastrous consequences in medical applications. Although adversarial noises are usually generated by attack algorithms, white-noise-induced adversarial samples can exist, and therefore the threats are real. In this study, we propose a novel training method, named IMA, to improve CNN robustness against adversarial noises. During training, the IMA method increases the margins of training samples in the input space, i.e., moving CNN decision boundaries far away from the training samples to improve robustness. The IMA method is evaluated on publicly available datasets under strong 100-PGD white-box adversarial attacks, and the results show that the proposed method significantly improved image classification and segmentation accuracy on noisy data while keeping a high accuracy on clean data. We hope our approach may facilitate the development of robust applications in the medical field.

1. Introduction

Deep neural networks (DNNs), especially convolutional neural networks (CNNs), have become the first choice for automated image analysis due to their superior performance. However, recent studies have shown that DNNs are not robust to adversarial noises. Adversarial noise was first discovered by [49] and then explained by [22]. Adversarial noises can significantly affect robustness of DNNs for a wide range of image classification applications [3, 18, 23, 36]. DNN-based image segmentation can also be affected by adversarial noises because image segmentation is often realized by pixel classification.

The COVID-19 pandemic has caused the death of more than 1 million people [58]. A large-scale study in China shows that CT had higher sensitivity for the diagnosis of

COVID-19 as compared with initial reverse-transcription polymerase chain reaction (RT-PCR) from swab samples [2]. As reviewed in [46], many DNN models for COVID-19 diagnosis from CT images have been developed and achieved very high classification accuracy. However, none of these studies [46] considered DNN robustness against adversarial noises. We modified a Resnet-18 model [24] and trained it on a public COVID-19 CT image dataset [48], and then the model robustness is tested (details in section 3.3). Fig. 1 shows a CT image (denoted by x) of a lung that was infected by COVID-19 and correctly classified as infected. After adding a small amount of noise δ to the image x , the noisy image $x + \delta$ is classified as uninfected. On the test set, although the model achieved $\geq 95\%$ accuracy on original clean images, its accuracy dropped to zero on small noise levels. This non-robust model clearly cannot be used in real clinical applications. Researchers have been working on DNN adversarial robustness from different aspects [1, 5, 7, 9, 10, 14, 17, 19–21, 27, 28, 32, 33, 39, 41, 44, 45, 54, 56, 59, 60, 63, 64].

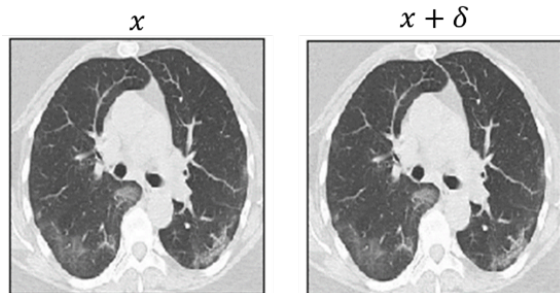


Figure 1. An example of clean and noisy images.

There are mainly two categories of adversarial attacks: white-box attack [8, 22, 31, 35] and black-box attack [11, 25]. For a white-box attack, the attacker knows everything about the DNN model to be attacked. For a black-box attack, the attacker only can use the DNN as a black-box (i.e., send an input to the DNN and get an output from the DNN, not

knowing anything else). From the perspective of defense, we should consider the worst-case scenario: white-box attack. Researchers have explored many ideas to improve robustness, but many of those have been shown to be ineffective [50, 51]. A general and effective strategy is adversarial training [4, 12, 15, 22, 35, 37, 57], and the basic idea is to use adversarial attack algorithms to generate noisy samples and add those samples to the training set. Through adversarial training, a DNN model can learn from the noisy samples and become robust to noises. Vanilla adversarial training [22, 31] is straightforward but problematic. It wrongly assumes that the perturbation is a fixed constant for all training samples. However, every sample may have different intrinsic robustness [12]. Generative adversarial training has been directly applied to improve robustness; however, it can only defend against black-box attack [55].

In this paper, we propose a novel adversarial training method, Increasing-Margin Adversarial (IMA) Training, to improve DNN robustness (our contribution-1). Our method aims to increase margins of training samples by moving decision boundaries far away from the samples gradually to improve robustness. We evaluated our method on datasets with 100-PGD white-box attack and compared it with the other six adversarial defense methods for image classification tasks. The results show that our proposed method can improve DNN robustness while keeping a satisfactory accuracy on clean data, better than MMA [15] (a state-of-the-art method). We also demonstrate that our IMA method can be used not only for image classification tasks but also for image segmentation tasks (our contribution-2).

2. Methodology

2.1. Adversarial Attack and Neural Network Robustness

To evaluate the robustness of different adversarial training methods, we used projected gradient descent (PGD) [31, 35] to generate adversarial noises, which is widely used for method evaluation [50, 51]. For the convenience of the reader, we briefly describe PGD: Let x denote an input sample and y be the true class label. Let $J(x)$ denote the scalar objective function of PGD, which could be the cross-entropy loss function or other classification loss functions. Let δ denote the adversarial noise, and its magnitude is ε which is measured by the vector L_p norm of δ , i.e., $\varepsilon = \|\delta\|_p$, where p is inf or 2 usually. PGD adds noises to x iteratively:

$$x_{(i)} = \text{clip}(x_{(i-1)} + \eta \cdot h(J'(x_{(i-1)}))) \quad (1)$$

where η is step size, $J'(x) = \frac{\partial J}{\partial x}$, and i is iteration index. $x_{(0)} = x + \xi$, where ξ is random noise with $\|\xi\|_p \leq \varepsilon$. The clip operation in Eq.(1) ensures that $\|x_{(i)} - x\|_p \leq$

ε (called ε -ball). If x is an image, the clip operation also ensures that pixel values stay within the feasible range (e.g. 0 to 1). If L -inf norm is used, $h(J')$ is the sign function; and if L 2 norm is used, then $h(J')$ normalizes J' by its L 2 norm. The total adversarial noise is $\delta = x_{(N_{PGD})} - x$, and N_{PGD} is the number of iterations. η is usually set to $\alpha \cdot \varepsilon / N_{PGD}$, and therefore the algorithm may sweep the ε -ball α times ($\alpha \geq 1$) within N_{PGD} iterations. By adding the adversarial noise δ to the input x , the objective function $J(x + \delta)$ will be significantly larger than $J(x)$, leading to wrong classification of the noisy sample $x + \delta$.

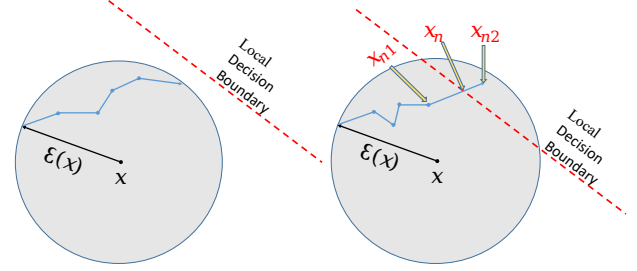


Figure 2. Left: case-0 in BPGD; Right: case-1 in BPGD. Please zoom in for better visualization.

It is easy to understand the robustness issue through Eq.(1) and Fig. 2. Given a trained classifier, if a sample x is very close to the decision boundary of the classifier, then one could add a small noise δ to x such that $x + \delta$ goes across the decision boundary and is wrongly classified. As shown in section 3, using standard training with cross-entropy loss and clean data, the decision boundaries of the trained classifier will often be very close to the samples; as a result, the accuracy can drop to zero upon very small noises.

To improve robustness, vanilla adversarial training [22, 31] based on PGD can be used: given the maximum noise level $\varepsilon = \varepsilon_{max}$, generate a noisy sample $x_\varepsilon = PGD(x, y, \varepsilon)$ for every clean sample x in training set; use the clean samples and noisy samples together to train the model. The loss function is given in [22]:

$$L_{adv} = (L_{ce}(x, y) + L_{ce}(x_\varepsilon, y)) / 2 \quad (2)$$

In practice, the loss is accumulated over each mini-batch. L_{ce} is the cross-entropy loss. As shown in the experiments, the vanilla adversarial training is very sensitive to the user-defined noise level ε_{max} .

2.2. Increasing-Margin Adversarial (IMA) Training

We developed a novel method, Increasing-Margin Adversarial (IMA) training, to enhance DNN classifier robustness. As its name indicates, IMA is a type of adversarial training: it generates noisy samples and trains a DNN

model on clean and noisy samples. IMA algorithms are significantly different from the other adversarial training algorithms.

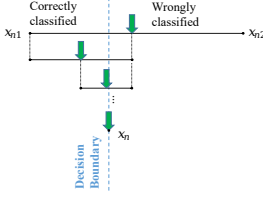


Figure 3. Binary search in BPGD.

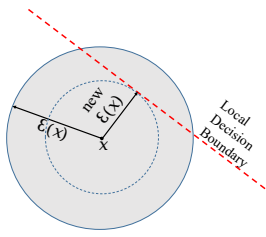


Figure 4. Shrink Margin.

IMA training includes two alternating sub-processes: Algorithm 1 to compute loss and update the DNN model, and Algorithm 2 to update margin estimation. In Algorithm 1, by minimizing the loss on clean and noisy data, the model will reach a balance between robustness and accuracy on clean data. In Algorithm 2, the sample margins are updated after each epoch. These estimated margins are used for generating noisy samples for training the model in the next epoch.

Algorithm 1 compute loss and update model in an epoch

Input: $S = (x, y)$ is the training set, containing pairs of clean sample x and true label y . f is the DNN model and $\hat{y} = f(x)$. \mathcal{E} is an array containing the estimated margins of individual training samples. β is a scalar coefficient. In a batch, X contains samples and Y contains class labels.

Output: updated model f after this training epoch

Process:

- 1: **for** Batch data X and Y in S **do**
- 2: Run model f to classify the samples and divide the samples into two groups, wrongly-classified X_0, Y_0 and correctly-classified X_1, Y_1 where $X = X_0 \cup X_1$ and $Y = Y_0 \cup Y_1$
- 3: Get noisy samples $X_n = BPGD(X_1, Y_1, \mathcal{E}(X_1))$ and classify them $\hat{Y}_n = f(X_n) \cdot \mathcal{E}(X_1)$ is a sub-array of \mathcal{E} , containing the estimated margins of samples in X_1 . $BPGD$ is described in Algorithm 3.
- 4: Compute the loss L :
- 5: $L_0 = \text{cross_entropy}(f(X_0), Y_0)$ (take sum)
- 6: $L_1 = \text{cross_entropy}(f(X_1), Y_1)$ (take sum)
- 7: $L_2 = \text{cross_entropy}(f(X_n), Y_1)$ (take sum)
- 8: $L = ((1 - \beta) \cdot (L_0 + L_1) + \beta \cdot L_2) / \text{batch_size}$
- 9: Back-propagate from L and update the model f
- 10: **end for**

Our IMA method tries to generate adversarial samples on decision boundaries as much as possible: adding too much noise to a training sample may lead to low accuracy on clean samples, but adding too little noise may have no effect on robustness. Since the distance between a training sample and a decision boundary is different for different training samples, the noises added to the training samples have different magnitudes (i.e., vector norms). The rationale for doing so is discussed in section 2.3. Here, the margin of a sample is the minimum distance between the sample and the decision boundaries. It is difficult to compute the exact margin for a sample in a high dimension space, and therefore we can only estimate it.

Algorithm 2 update margin estimation after an epoch

Input: $S = (x, y)$ is the training set. f is the DNN model and $\hat{y} = f(x)$. \mathcal{E} is an array of the estimated margins of training samples. $\mathcal{E}(x)$ is the estimated margin of x . Δ_ϵ is margin expansion step size. ϵ_{max} is the maximum noise level, i.e., the allowed maximum margin.

Output: updated \mathcal{E}

Process:

- 1: **for** each sample x and y in S **do**
- 2: Get noisy sample $x_n = BPGD(x, y, \mathcal{E}(x))$ (From Algorithm 1)
- 3: **if** x_n is on decision boundary (not None, which means $\mathcal{E}(x)$ is larger than what it should be) **then**
- 4: Update $\mathcal{E}(x) = (||x - x_n||_p + \mathcal{E}(x))/2$ (shrink)
- 5: **else**
- 6: Update $\mathcal{E}(x) = \mathcal{E}(x) + \Delta_\epsilon$ (expand)
- 7: **end if**
- 8: **end for**
- 9: Clip every element of \mathcal{E} into the range of 0 to ϵ_{max}

Note: Every $\mathcal{E}(x)$ is initialized to be Δ_ϵ which can be set to ϵ_{max} divided by the number of adversarial training epochs. The algorithm runs in mini-batches.

Algorithm 3 (BPGD): generate noisy samples

Input: : a sample x with class label y , the estimated margin ϵ of x , and the model $f \cdot N_{PGD}$ is the number of iterations in PGD. N_{binary} is the number of iterations in binary search.

Output: $x_n = BPGD(x, y, \epsilon)$

Process:

- 1: Run the standard $PGD(x, y, \epsilon)$ and obtain a sequence of noisy samples (N_{PGD} samples)
- 2: Classify those noisy samples using the model f
- 3: **if** all of the noisy samples are correctly-classified (case-0 in Fig.2) **then**
- 4: **return** None (x_n is None and will be ignored)
- 5: **else**
- 6: (case-1 in Fig.2) Find x_{n1} and x_{n2} , two adjacent samples in the sequence. x_{n1} is correctly-classified and x_{n2} is wrongly-classified. Thus, x_{n1} and x_{n2} are close to the decision boundary.
- 7: Run binary search along the straight-line segment between x_{n1} and x_{n2} in order to find x_n on the decision boundary (Fig. 3)
- 8: **return** x_n
- 9: **end if**

Note: 1. It is unnecessary to store the whole sequence. The algorithm runs in mini-batches. 2. N_{binary} is set to 10, which is constant. So, this binary search's time complexity is $O(1)$.

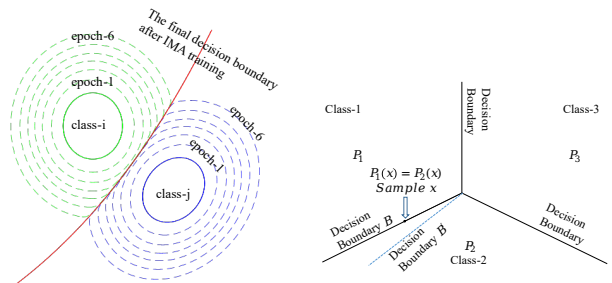


Figure 5. Left: Equilibrium State; Right: Three-class Scenario.

We developed Algorithm 3, named BPGD, to find noisy samples on decision boundaries. At the very beginning of the IMA training process, the margins of the training samples are initialized to a small number equal to margin expansion step size in Algorithm 2. Intuitively, during IMA training, the margin of a training sample keeps increasing as if a ball is expanding (the ball center is the sample x , and the radius is the margin $\mathcal{E}(x)$; it is called ϵ -ball), until the ball of the sample x collides with the ball of another sample

x' in a different class. When the two balls collide and therefore a local decision boundary is formed, Algorithm 2 will prevent them from further expansion by refining/shrinking margins (Fig. 4). In section 2.3, we will show that an equilibrium state may exist (Fig. 5) under which the margins of the samples are maximized.

2.3. the Equilibrium State

We can show that on certain conditions, an equilibrium state (Fig. 5-Left) exists under which the margins of the samples are maximized. To simplify the discussion, we assume there are three classes and three decision boundaries between classes (Fig. 5-Right). The softmax output of the neural network model f has three components: P_1 , P_2 and P_3 corresponding to the three classes. If a point (i.e., a sample) x is on the decision boundary B_{ij} between class- i (c_i) and class- j (c_j), then $P_i(x) = P_j(x)$. The mathematical expectation of the cross-entropy loss of the noisy samples (L_2 in Algorithm 1) is:

$$E = \mathbf{E}_{X_n \in c_1} (-\log(P_1(X_n))) + \mathbf{E}_{X_n \in c_2} (-\log(P_2(X_n))) + \mathbf{E}_{X_n \in c_3} (-\log(P_3(X_n))) \quad (3)$$

The IMA method puts the noisy samples on the decision boundaries, thus:

$$\mathbf{E}_{X_n \in c_1} (-\log(P_1(X_n))) = \mathbf{E}_{X_n \in c_1, B_{12}} (-\log(P_1(X_n))) + \mathbf{E}_{X_n \in c_1, B_{13}} (-\log(P_1(X_n))) \quad (4)$$

$$\mathbf{E}_{X_n \in c_2} (-\log(P_2(X_n))) = \mathbf{E}_{X_n \in c_2, B_{12}} (-\log(P_2(X_n))) + \mathbf{E}_{X_n \in c_2, B_{23}} (-\log(P_2(X_n))) \quad (5)$$

$$\mathbf{E}_{X_n \in c_3} (-\log(P_3(X_n))) = \mathbf{E}_{X_n \in c_3, B_{13}} (-\log(P_3(X_n))) + \mathbf{E}_{X_n \in c_3, B_{23}} (-\log(P_3(X_n))) \quad (6)$$

If the noisy samples (random variables) $X_n \in c_i$ and $X_n \in c_j$ have the same spatial distribution on the decision boundary B_{ij} between the two classes, Eq.(3) can be simplified to

$$E = \mathbf{E}_{X_n \in B_{12}} + \mathbf{E}_{X_n \in B_{23}} + \mathbf{E}_{X_n \in B_{13}} \quad (7)$$

where

$$\begin{aligned} & \mathbf{E}_{X_n \in B_{ij}} \\ &= \mathbf{E}_{X_n \in B_{ij}} (-\log(P_i(X_n)) - \log(P_j(X_n))) \\ &= \mathbf{E}_{X_n \in B_{ij}} (-\log(P_i(X_n) P_j(X_n))) \\ &\geq \mathbf{E}_{X_n \in B_{ij}} \left(-\log \left(\frac{P_i(X_n) + P_j(X_n)}{2} \right)^2 \right) \end{aligned} \quad (8)$$

E reaches the minimum when $P_i(X_n) = P_j(X_n)$.

The analysis shows that the loss of noisy samples will increase if the decision boundaries of the model f change from the current state. Thus, when the loss ($L_0 + L_1$) on clean data is minimized and noisy samples are generated on

the decision boundaries, an equilibrium is reached under the condition that noisy samples have the same spatial distribution on the decision boundaries between classes. This analysis provides the rationale that our IMA method puts the noisy/adversarial samples on decision boundaries as much as possible, which is significantly different from the theory of the MMA method [15].

2.4. Comparison with MMA

The MMA method [15], which is a state-of-the-art adaptive adversarial training method, is based on sample-wise adversarial noises (margins) estimated by PGD attack [35] directly. However, its estimation has a problem (see Fig. 6). PGD attack searches within an epsilon ball. Once it reaches a point x_n on the "true" decision boundary, the MMA treats the distance between the point x_n and the original/clean data sample x as the estimated margin (the dashed line in Fig. 6 (right)), which is very likely to be much larger than the real margin. In our proposed method, by gradually expanding the epsilon ball, the estimated margin is closer to the real margin (the dashed line in Fig. 6 (left)). This can be shown by the experiment of COVID-19 CT image classification. The Fig. 8 shows the distributions of the estimated margins. MMA significantly overestimated the margins. Details can be seen in the COVID-19 CT classification section. IMA largely relieves the margin overestimation problem. As a result, in the evaluations on image classification in this paper, IMA outperforms MMA in general.

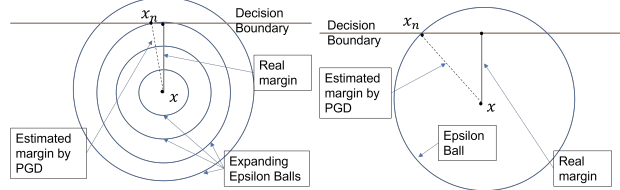


Figure 6. IMA margin estimations (left), and MMA margin estimations (right)

3. Experiments of Image Classification

We applied the IMA method on classification for 5 DNNs on 5 different datasets: Moons, Fashion-MNIST, SVHN, CIFAR10 and COVID-19 CT. To describe the DNNs, we use "COV (a, b, c, d, e)" to represent a convolution layer with "a" input channels, "b" output channels, kernel size of "c", stride of "d" and padding of "e"; "Linear (f, g)" to denote a linear layer with input size of "f" and output size of "g"; "IN" to denote instance normalization; "LN" to denote layer normalization, and "LR" to denote leaky ReLU.

To obtain the baseline performance, each DNN was trained with cross-entropy loss on clean data, denoted by

“ce”. To evaluate the performance, we compared our method with other adversarial training methods, including: (1) 20-PGD ($N_{PGD}=20$ and $\alpha=4$) based vanilla adversarial training with noise level ε , denoted by “adv ε ” [22, 31] ; (2) TRADES in [65]; (3) MMA in [15]; (4) DDN in [43]; (5) FAT in [66]; (6) GAIRAT in [67]. MMA is a state-of-the-art method, and TRADES was state-of-the-art at the time of its publication. N_{PGD} of IMA is 20. We used PGD to evaluate the robustness of the methods, which is widely used for method evaluation [34, 51]. The number of PGD iterations is 100 to ensure a strong attack, and it is called 100-PGD. To further enhance the stability of testing result, each 100-PGD runs twice using MarginalLoss and CrossEntropyLoss respectively, which is implemented in [16]<https://github.com/BorealisAI/advertorch>. For simplicity, we use “**clean accuracy**” to refer to the accuracy on clean data, and “**noisy accuracy**” to refer to the accuracy on noisy data. The details of the experiments are in Appendix G. Because of the nature of IMA, it does not have significant robust overfitting problem [29, 42] (see Appendix H.1). Blackbox-attack evaluation with SPSA [51] is in Appendix H.2, which shows there is no gradient obfuscation in IMA.

3.1. Evaluation on Moons dataset

The Moons dataset is available in sk-learn [40]. There are two classes of 2D points in the dataset. The training set has 20000 samples, the validation set has 2000 samples, and the test set has 2000 samples. The neural network structure is Linear(2, 32)-LR-Linear(32, 64)-LN-LR-Linear(64, 128)-LN-LR-Linear(128, 2). The purpose of this evaluation is to visualize the decision boundaries of the models trained by different adversarial training methods. To measure robustness on the test set, adversarial samples on different noise levels (defined by L2 norm) are generated by the 100-PGD.

From Fig. 7, our method IMA is better than the other methods, and its decision boundary is close to the “middle line” of the two classes. The results of TRADES and adv0.3 are very similar: the decision boundary is far away from most of the red dots. We note that 0.3 is roughly the distance between two classes.

3.2. Evaluation on Fashion-MNIST, SVHN and CIFAR10 datasets

We used Fashion-MNIST dataset [62] instead of MNIST which is too easy. The dataset contains 28×28 grayscale images in 10 classes (shirts, shoes, etc.). The network structure is COV(1, 64, 5, 2, 2)-LR-COV(64, 128, 5, 2, 2)-IN-LR-COV (128, 256, 5, 2, 2)-IN-LR-COV (256, 512, 4, 1, 0)-Flatten-LN-LR-Linear(512, 10). The results are shown in Table. 1. IMA outperformed MMA, FAT, and GAIRAT. DDN performed slightly better than IMA on the noise levels of 2.0 and 3.0, but it had a lower clean accuracy. We note

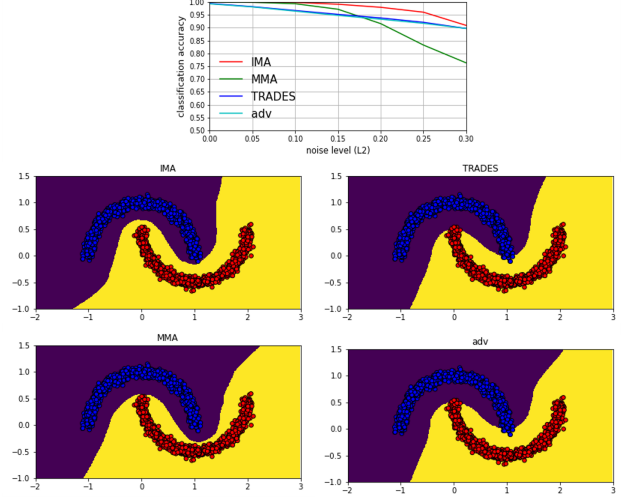


Figure 7. Results on Moons dataset (L2 norm in 100-PGD).

Noise	0.0	0.5	1.0	2.0	3.0
ce	91.17	25.12	0.33	0.0	0.0
IMA	88.98	80.73	69.64	47.62	32.42
MMA	89.26	80.70	69.27	46.17	26.51
FAT	86.09	79.08	67.21	34.82	10.79
GAIRAT	83.11	69.53	53.24	20.41	2.15
DDN	86.21	78.53	68.80	49.47	34.67
TRADES	91.76	61.03	49.77	34.25	18.75
adv1.0	90.86	80.96	65.49	27.26	5.13
adv3.0	91.72	64.10	58.59	47.54	33.25
adv5.0	91.48	48.51	41.61	30.11	21.21

Table 1. Classification accuracy on Fashion-MNIST (L2 norm in 100-PGD).

Noise	0.0	0.1	0.25	0.5	1.0
ce	93.20	75.88	41.25	11.85	0.92
IMA	89.69	85.01	76.82	60.50	31.90
MMA	87.65	83.22	75.18	59.74	32.15
FAT	88.01	81.94	70.24	42.76	12.12
GAIRAT	91.66	84.90	68.25	36.52	7.31
DDN	86.95	82.17	73.85	58.43	31.40
TRADES	87.30	80.76	69.03	45.81	12.38
adv0.5	89.86	84.90	75.08	53.90	20.62
adv1.0	87.30	82.84	75.04	58.87	26.54
adv2.0	86.63	81.75	71.95	54.58	28.83

Table 2. Classification accuracy on SVHN (L2 norm in 100-PGD).

that clean accuracy should not be sacrificed too much in order to achieve high robustness (i.e., noisy accuracy). “adv ε ” is very sensitive to the parameter ε .

Noise	0.0	0.5	1.0	1.5
ce	94.92	0.98	0.0	0.0
IMA	88.22	65.82	39.80	20.50
MMA	88.02	66.19	37.80	15.61
FAT	87.11	52.02	15.89	3.01
GAIRAT	86.75	49.49	16.35	3.45
DDN	89.05	66.51	39.02	16.63
TRADES	84.98	54.61	21.48	6.23
adv0.5	89.10	65.61	33.23	11.29
adv1.0	83.25	66.69	46.11	26.16
adv1.5	75.80	62.74	48.35	33.80

Table 3. Classification accuracy on CIFAR10 (L2 norm in 100-PGD).

We also used SVHN dataset which contains 32×32 color images of 0 ~ 9 digits [38]. The network structure is COV(3, 32, 3, 1, 1)-LR-COV(32, 32, 3, 2, 1)-IN-LR-COV(32, 64, 3, 1, 1)-IN-LR-Conv2d(64, 64, 3, 2, 1)-IN-LR-COV(64, 128, 3, 1, 1)-IN-LR-Conv2d(128, 128, 3, 2, 1)-IN-LR-COV(128, 256, 4, 1, 0)-Flatten-LN-LR-Linear(256, 10). The results are shown in Table. 2. IMA outperformed all the other methods.

Then, we used CIFAR10 dataset which contains 60000 32×32 color images in 10 classes [30]. The network is WRN-28-4 [15]. The results are shown in Table. 3. IMA outperformed MMA, FAT, GAIRAT, and TRADES. DDN performed slightly better than IMA on the noise levels of 0 and 0.5. DDN uses 100 iterations to find adversarial samples, which is almost equivalent to using 100-PGD for adversarial training, and this is the reason that DDN performed better on this dataset. In contrast, IMA uses 20-PGD internally, which has a much smaller computation cost. “adv ε ” is very sensitive to the parameter ε .

3.3. Application of COVID-19 detection from CT images

We used a public COVID-19 CT image dataset [48], which was collected from patients in hospitals from Sao Paulo, Brazil. It contains 1252 CT scans (2D images) that are positive for COVID-19 infection and 1230 CT scans (2D images) for patients non-infected by COVID-19, 2482 CT scans in total. From infected cases, we randomly selected 200 samples for testing, 30 for validation, and 1022 for training. From the uninfected cases, we randomly selected 200 for testing, 30 for validation and 1000 for training. Each image is resized to 224×224 . Since there is no pixel segmentation mask in the dataset, we can only perform classification for COVID-19 detection on the image level. We modified the output layer of the Resnet-18 model [24] for the binary classification task: uninfected (label 0) vs infected (label 1), and we also replaced batch normalization

Noise	0	1	3	5	10	30
ce	95.75	9.98	0.0	0.0	0.0	0.0
IMA	91.25	90.25	87.75	83.25	57.00	0.0
MMA	89.00	88.50	84.25	80.00	57.50	0.0
DDN	90.25	88.50	84.75	78.75	59.75	0.0
TRADES	97.25	12.75	10.25	11.00	19.75	48.75
GAIRAT	92.50	88.25	72.50	50.25	12.50	0.0
FAT	90.00	88.00	81.50	64.25	16.00	0.0
adv10	93.50	92.25	89.50	83.50	53.50	0.0
adv20	95.25	25.50	20.00	21.50	22.50	3.00
adv30	85.25	6.25	1.50	2.00	5.00	23.00

Table 4. Classification accuracy on COVID-19 CT image dataset (L2 norm in 100-PGD).

with instance normalization because it is known that batch normalization is not stable for small batch-size [61]. As shown in the previous studies [46], infected regions in the images have a special pattern called ground-glass opacity.

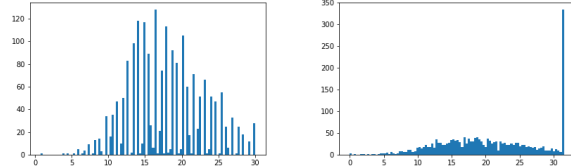


Figure 8. IMA estimated margin distribution (left), and MMA estimated margin distribution (right). MMA significantly overestimated the margins.

Details of this experiment can be seen in Appendix G. To measure robustness on the test set, adversarial samples on different noise levels (L2 norm) are generated by the 100-PGD. From Table. 4, the results show that no single method performed the best on all noise levels. IMA and “adv 10” had very similar performance, and IMA performed better than MMA.

Fig. 8 shows the distribution of estimated margins of all the training samples, where x-axis shows the magnitude of margins (in L2 norm) and y-axis shows the frequency. From Fig. 8 (right), it can be seen that about 1/6 of the estimated margins from MMA are larger than 30, which means about 1/6 of samples should have been free of influence of noises with magnitude less than 30. However, the accuracy of MMA on the noise level of 30 is 0. The results show that MMA significantly overestimated the margins of samples because MMA does not consider the equilibrium (Fig.5) between classes. From Fig. 8 (left), the problem of margin overestimation was relieved in IMA, which is the reason that IMA outperforms MMA in all the evaluations in this paper. It also can be seen that the vanilla adversarial

training (“adv ε ”) is good when the training noise level ε is chosen “properly”. A straightforward way to find a good ε would be running grid-research and evaluating the performance on the validation set, which is computationally expensive. The margin distribution (Fig. 8(left)) estimated by our method IMA indicates a good $\varepsilon = 10$ for vanilla adversarial training. This is because 10 is just smaller than the majority of the margins, which will not make the noisy samples to go cross the true decision boundary.

4. Extension of IMA for Medical Image Segmentation

The IMA algorithm can also be applied to improve DNN robustness for image segmentation tasks. For image segmentation tasks, we reformulate a segmentation task as a classification task. Since Dice index is often used to evaluate segmentation performance, a segmentation can be considered “correct” if $\text{Dice} > \text{threshold}$, and “wrong” otherwise, which is binary classification to classify the segmentation output. In the experiments, this Dice threshold is set to 60% for all of the datasets because a Dice score higher than 60% is considered “good” for medical applications [6, 13, 52, 53]. For non-medical images, there is no consensus about a good Dice score, which is the reason we used medical images.

In the experiments, we applied the IMA method on a self-configuring DNN, named nnUnet [26]. The nnUnet can automatically configure itself, including preprocessing, network architecture, training, and post-processing for the input dataset. In the experiment, we selected three publically available datasets [26], which are Heart (D2), Hippocampus (D4) and Prostate (D5) [47]. Noise levels are measured by L2 norm. Because image segmentation robustness is an underexplored area, we compared only three methods: (1) the proposed IMA, denoted by “IMA”; (2) the 20-PGD based vanilla adversarial training with training noise level of ε , denoted be “adv ε ” [22] ; (3) the nnUnet, which is trained on clean data, denoted by “nnUnet”. For evaluation, the adversarial attack is 100-PGD. For these methods, we used the original loss function in [26] as the replacement of cross-entropy loss. The details are in Appendix. G.

In the experiments, two metrics are used to evaluate the performance. The first one is “Total Voxel Dice Index (TVDI)”, which is given by:

$$\text{TVDI} = \frac{2 \times \sum_i^n \text{TP}_i}{2 \times \sum_i^n \text{TP}_i + \sum_i^n \text{FP}_i + \sum_i^n \text{FN}_i} \quad (9)$$

where the n is the number of samples in the testset, TP_i is the number of voxels in true positive area of the sample i , FP_i is the number of voxels in false positive area of the sample i and FN_i is the number of voxels in false negative area of the sample i . The second metric is “Average Dice

Noise	0	5	15	25
nnUnet	92.46	69.12	2.01	0.0
IMA	85.34	80.23	69.34	56.33
adv5	87.23	80.78	60.12	35.01
adv15	84.21	80.15	67.48	50.98
adv25	80.44	76.11	68.19	58.90

Table 5. Segmentation results on D2: Total Voxel Dice Index.

Noise	0	5	15	25
nnUnet	80.01	51.69	2.17	0.0
IMA	75.43	70.16	55.79	44.06
adv5	75.12	65.43	46.31	23.78
adv15	72.15	66.34	53.36	38.12
adv25	66.78	61.65	52.67	43.79

Table 6. Segmentation results on D2: Average Dice Index.

Index (ADI)”, whose formula is:

$$\text{ADI} = \sum_i^n \frac{2 \times \text{TP}_i}{2 \times \text{TP}_i + \text{FP}_i + \text{FN}_i} \times \frac{1}{n} \quad (10)$$

TVDI is the metric used in the original paper of nnUnet (Isensee et al. 2021). We used it to show that our results on clean data are similar to the reported results in (Isensee et al. 2021). However, in the TVDI metric, the individual samples do not have equal weights. We introduced ADI, a better metric to equally weight the samples, which also highlights the differences between the three methods. For simplicity, we use “clean TVDI/ADI” to refer to the metric score on clean data, and “noisy TVDI/ADI” to refer to the metric score on noisy data.

4.1. Evaluation on Heart (D2)

This dataset has 20 labeled 3D images: 16 for training, 1 for validation and 3 for testing. The median shape of each 3D image is $115 \times 320 \times 232$, where 115 is the number of slices. In this experiment, we only focused on 2D segmentation, so each slice is an input sample of the model. The batch size (40), patch size (320×256) and network structure are self-configured by nnUnet for this dataset.

From Table. 5, “nnUnet” has the weakest defense against adversarial attack, whose TVDI score drops to almost 0 at the noise level of 15. It can be seen that “adv5” has a high clean TVDI (0.87), but is not robust enough (its TVDI score drops very fast as the noise level goes up). “adv25” is very robust as its TVDI score drops slowliest when the noise level goes up), but its clean TVDI score is more than 10% lower than the score of the original “nnUnet”, which means the noise level for training is so large that it has significantly affected the original model’s functionality. “adv15” is not

Noise	0	1	5	10	15
nnUnet	86.45	78.13	15.00	0.0	0.0
IMA	82.19	80.14	72.49	56.27	32.01
adv1	85.36	82.01	60.89	20.98	2.03
adv5	83.21	81.90	70.68	50.79	19.98
adv15	79.89	78.11	69.56	50.67	27.76

Table 7. Segmentation results on D4: Total Voxel Dice Index.

Noise	0	1	5	10	15
nnUnet	75.23	64.10	9.00	0.0	0.0
IMA	74.01	72.06	64.32	49.11	26.95
adv1	73.95	69.05	48.83	15.04	0.91
adv5	70.56	69.05	58.16	37.85	16.17
adv15	69.23	66.80	58.23	41.12	22.49

Table 8. Segmentation results on D4: Average Dice Index.

as robust as “IMA” in general. The results show the weakness of vanilla adversarial training: very large training noise will destroy the model while very small training noise cannot make the model robust enough. As revealed by the AVI metric (Table. 6), IMA has a significantly better performance than the other methods.

4.2. Evaluation on Hippocampus (D4)

This D4 dataset has 260 labeled 3D images: 208 for training, 17 for validation and 35 for testing. The median shape of each 3D image is $36 \times 50 \times 35$, where 36 is the number of slices and 50×35 is the input size. The batch size (366), patch size (56×40) and network structure are self-configured by nnUnet for this dataset.

From Table. 7, “nnUnet”’s TVDI score drops to almost 0 at the noise level of 10, which shows the 100-PGD is a very strong attack. It can be seen that “adv1” has a good clean TVDI score (85%), but is not robust enough. “adv15” is very robust but has the lowest clean TVDI score (< 80%). “adv5” has a very high TVDI score on clean data but is not as robust as “IMA”. As revealed by the ADI metric in Fig. 8, IMA has the best performance.

4.3. Evaluation on Prostate (D5)

This D5 dataset has 32 labeled 3D images: 25 for training, 2 for validation and 5 for testing. The median shape of each 3D image is $20 \times 320 \times 319$, where 20 is the number of slices and 320×319 is the input size. The batch size (32), patch size (320×320) and network structure are self-configured by nnUnet for this dataset.

As shown in Table. 9, although the clean TVDI scores of “IMA”, “adv20” and “adv10” are almost the same (around 0.73), “adv20” and “adv10” are not as robust as “IMA”.

Noise	0	10	20	40
nnUnet	80.89	37.14	18.09	7.01
IMA	72.23	66.14	59.15	43.45
adv40	70.76	63.18	54.67	38.13
adv20	72.46	65.34	56.78	38.19
adv10	73.12	61.67	50.43	28.23

Table 9. Segmentation results on D5: Total Voxel Dice Index.

Noise	0	10	20	40
nnUnet	74.34	30.14	13.90	4.08
IMA	66.80	61.15	55.41	38.01
adv40	65.49	56.13	45.78	28.90
adv20	65.89	56.34	44.76	27.86
adv10	66.04	54.48	39.96	21.85

Table 10. Segmentation results on D5: Average Dice Index.

Also, “adv40” is not as good as “IMA” on both clean and noisy data. As shown by the ADI metric in Table. 10, IMA has the best performance.

5. Conclusion

In this study, we proposed a novel Increasing-Margin Adversarial (IMA) training method to improve the robustness of DNNs for image classification and segmentation tasks. Our method aims to increase the margins of the training samples to improve DNN robustness against adversarial attacks. By increasing the margins of the training samples gradually, IMA relieved the margin overestimation problem in MMA, a state-of-the-art adaptive adversarial training method based on sample-wise adversarial noises (margins) estimated by PGD attack. The experiment results show that our method IMA outperformed MMA and significantly improved DNN classification accuracy on noisy data while keeping a relatively high accuracy on clean data. Also, the experiment results show that our method can be applied to improve DNN robustness for image segmentation tasks. Although IMA had a good performance on the COVID-19 CT images classification task, there is still a large room to apply IMA to other domains, especially medical applications. We hope our approach may facilitate the development of robust DNNs for more medical applications in the future.

Note: 1. the appendix is available at <https://github.com/SarielMa/IMA>; 2. the code will be released after this paper is published.

References

- [1] Akshay Agarwal, Mayank Vatsa, and Richa Singh. Role of optimizer on network fine-tuning for adversarial robust-

ness (student abstract). In *AAAI*, pages 15745–15746. AAAI Press, 2021. 1

[2] Tao Ai, Zhenlu Yang, Hongyan Hou, Chenao Zhan, Chong Chen, Wenzhi Lv, Qian Tao, Ziyong Sun, and Liming Xia. Correlation of chest ct and rt-pcr testing in coronavirus disease 2019 (covid-19) in china: a report of 1014 cases. *Radiology*, page 200642, 2020. 1

[3] Naveed Akhtar and Ajmal Mian. Threat of adversarial attacks on deep learning in computer vision: A survey. *IEEE Access*, 6:14410–14430, 2018.

[4] Anish Athalye, Nicholas Carlini, and David Wagner. Obfuscated gradients give a false sense of security: Circumventing defenses to adversarial examples. In Jennifer Dy and Andreas Krause, editors, *ICML*, volume 80 of *Proceedings of Machine Learning Research*, pages 274–283. PMLR, 10–15 Jul 2018. 2

[5] Pranjal Awasthi, George Yu, Chun-Sung Ferng, Andrew Tomkins, and Da-Cheng Juan. Adversarial robustness across representation spaces. In *Proceedings of the IEEE/CVF Conference on Computer Vision and Pattern Recognition*, pages 7608–7616, 2021. 1

[6] John J Bartko. Measurement and reliability: statistical thinking considerations. *Schizophrenia bulletin*, 17(3):483–489, 1991. 7

[7] Tuan-Anh Bui, Trung Le, He Zhao, Paul Montague, Olivier Y. de Vel, Tamas Abraham, and Dinh Phung. Improving ensemble robustness by collaboratively promoting and demoting adversarial robustness. In *AAAI*, pages 6831–6839. AAAI Press, 2021. 1

[8] Nicholas Carlini and David Wagner. Towards evaluating the robustness of neural networks. In *2017 ieee symposium on security and privacy (sp)*, pages 39–57. IEEE, 2017. 1

[9] George Cazenavette, Calvin Murdock, and Simon Lucey. Architectural adversarial robustness: The case for deep pursuit. In *Proceedings of the IEEE/CVF Conference on Computer Vision and Pattern Recognition*, pages 7150–7158, 2021. 1

[10] Pin-Chun Chen, Bo-Han Kung, and Jun-Cheng Chen. Class-aware robust adversarial training for object detection. In *Proceedings of the IEEE/CVF Conference on Computer Vision and Pattern Recognition*, pages 10420–10429, 2021. 1

[11] Pin-Yu Chen, Huan Zhang, Yash Sharma, Jinfeng Yi, and Cho-Jui Hsieh. Zoo: Zeroth order optimization based black-box attacks to deep neural networks without training substitute models. In *Proceedings of the 10th ACM workshop on artificial intelligence and security*, pages 15–26, 2017. 1

[12] Minhao Cheng, Qi Lei, Pin-Yu Chen, Inderjit Dhillon, and Cho-Jui Hsieh. Cat: Customized adversarial training for improved robustness, 2020. 2

[13] Domenic V Cicchetti. Guidelines, criteria, and rules of thumb for evaluating normed and standardized assessment instruments in psychology. *Psychological assessment*, 6(4):284, 1994. 7

[14] Zhijie Deng, Xiao Yang, Shizhen Xu, Hang Su, and Jun Zhu. Libre: A practical bayesian approach to adversarial detection. In *Proceedings of the IEEE/CVF Conference on Computer Vision and Pattern Recognition*, pages 972–982, 2021. 1

[15] Gavin Weiguang Ding, Yash Sharma, Kry Yik Chau Lui, and Ruitong Huang. Mma training: Direct input space margin maximization through adversarial training. In *ICLR*, 2020. 2, 4, 5, 6

[16] Gavin Weiguang Ding, Luyu Wang, and Xiaomeng Jin. AdverTorch v0.1: An adversarial robustness toolbox based on pytorch, 2019. 5

[17] Andrew Elliott, Stephen Law, and Chris Russell. Explaining classifiers using adversarial perturbations on the perceptual ball. In *Proceedings of the IEEE/CVF Conference on Computer Vision and Pattern Recognition*, pages 10693–10702, 2021. 1

[18] Kevin Eykholt, Ivan Evtimov, Earlene Fernandes, Bo Li, Amir Rahmati, Chaowei Xiao, Atul Prakash, Tadayoshi Kohno, and Dawn Song. Robust physical-world attacks on deep learning visual classification. In *CVPR*, pages 1625–1634, 2018. 1

[19] Jiameng Fan and Wenchao Li. Adversarial training and provable robustness: A tale of two objectives. In *AAAI*, pages 7367–7376. AAAI Press, 2021. 1

[20] Tejas Gokhale, Rushil Anirudh, Bhavya Kailkhura, Jayaraman J. Thiagarajan, Chitta Baral, and Yezhou Yang. Attribute-guided adversarial training for robustness to natural perturbations. In *AAAI*, pages 7574–7582. AAAI Press, 2021. 1

[21] Chengyue Gong, Tongzheng Ren, Mao Ye, and Qiang Liu. Maxup: Lightweight adversarial training with data augmentation improves neural network training. In *Proceedings of the IEEE/CVF Conference on Computer Vision and Pattern Recognition*, pages 2474–2483, 2021. 1

[22] Ian Goodfellow, Jonathon Shlens, and Christian Szegedy. Explaining and harnessing adversarial examples. In *ICLR*, 2015. 1, 2, 5, 7

[23] Abigail Graese, Andras Rozsa, and Terrance E Boult. Assessing threat of adversarial examples on deep neural networks. In *ICMLA*, pages 69–74. IEEE, 2016. 1

[24] Kaiming He, Xiangyu Zhang, Shaoqing Ren, and Jian Sun. Deep residual learning for image recognition. In *CVPR*, pages 770–778, 2016. 1, 6

[25] Andrew Ilyas, Logan Engstrom, Anish Athalye, and Jessy Lin. Black-box adversarial attacks with limited queries and information. In *ICML*, pages 2137–2146. PMLR, 2018. 1

[26] Fabian Isensee, Paul F Jaeger, Simon AA Kohl, Jens Petersen, and Klaus H Maier-Hein. nnu-net: a self-configuring method for deep learning-based biomedical image segmentation. *Nature methods*, 18(2):203–211, 2021. 7

[27] Jinyuan Jia, Xiaoyu Cao, and Neil Zhenqiang Gong. Intrinsic certified robustness of bagging against data poisoning attacks. In *AAAI*, pages 7961–7969. AAAI Press, 2021. 1

[28] Shuai Jia, Yibing Song, Chao Ma, and Xiaokang Yang. Iou attack: Towards temporally coherent black-box adversarial attack for visual object tracking. In *Proceedings of the IEEE/CVF Conference on Computer Vision and Pattern Recognition*, pages 6709–6718, 2021. 1

[29] Hoki Kim, Woojin Lee, and Jaewook Lee. Understanding catastrophic overfitting in single-step adversarial training. In *AAAI*, 2021. 5

[30] Alex Krizhevsky, Geoffrey Hinton, et al. Learning multiple layers of features from tiny images. 2009. 6

[31] Alexey Kurakin, Ian Goodfellow, Samy Bengio, et al. Adversarial examples in the physical world, 2016. 1, 2, 5

[32] Xin Li, Xiangrui Li, Deng Pan, and Dongxiao Zhu. Improving adversarial robustness via probabilistically compact loss with logit constraints. In *AAAI*, pages 8482–8490. AAAI Press, 2021. 1

[33] Youwei Liang and Dong Huang. Large norms of CNN layers do not hurt adversarial robustness. In *AAAI*, pages 8565–8573. AAAI Press, 2021. 1

[34] Fangzhou Liao, Ming Liang, Yinpeng Dong, Tianyu Pang, Xiaolin Hu, and Jun Zhu. Defense against adversarial attacks using high-level representation guided denoiser. In *CVPR*, pages 1778–1787, 2018. 5

[35] Aleksander Madry, Aleksandar Makelov, Ludwig Schmidt, Dimitris Tsipras, and Adrian Vladu. Towards deep learning models resistant to adversarial attacks. In *ICLR*, 2018. 1, 2, 4

[36] Vahid Mirjalili and Arun Ross. Soft biometric privacy: Retaining biometric utility of face images while perturbing gender. In *IJCB*, pages 564–573. IEEE, 2017. 1

[37] Takeru Miyato, Shin-ichi Maeda, Masanori Koyama, and Shin Ishii. Virtual adversarial training: a regularization method for supervised and semi-supervised learning. *IEEE transactions on pattern analysis and machine intelligence*, 41(8):1979–1993, 2018. 2

[38] Yuval Netzer, Tao Wang, Adam Coates, Alessandro Bissacco, Bo Wu, and Andrew Y Ng. Reading digits in natural images with unsupervised feature learning. In *NIPS Workshop on Deep Learning and Unsupervised Feature Learning*, 2011. 6

[39] Kun-Peng Ning, Lue Tao, Songcan Chen, and Sheng-Jun Huang. Improving model robustness by adaptively correcting perturbation levels with active queries. In *AAAI*, pages 9161–9169. AAAI Press, 2021. 1

[40] Fabian Pedregosa, Gaël Varoquaux, Alexandre Gramfort, Vincent Michel, Bertrand Thirion, Olivier Grisel, Mathieu Blondel, Peter Prettenhofer, Ron Weiss, Vincent Dubourg, et al. Scikit-learn: Machine learning in python. *the Journal of machine Learning research*, 12:2825–2830, 2011. 5

[41] Arianna Rampini, Franco Pestarini, Luca Cosmo, Simone Melzi, and Emanuele Rodola. Universal spectral adversarial attacks for deformable shapes. In *Proceedings of the IEEE/CVF Conference on Computer Vision and Pattern Recognition*, pages 3216–3226, 2021. 1

[42] Leslie Rice, Eric Wong, and Zico Kolter. Overfitting in adversarially robust deep learning. In *ICML*, pages 8093–8104. PMLR, 2020. 5

[43] Jérôme Rony, Luiz G Hafemann, Luiz S Oliveira, Ismail Ben Ayed, Robert Sabourin, and Eric Granger. Decoupling direction and norm for efficient gradient-based l2 adversarial attacks and defenses. In *Proceedings of the IEEE/CVF Conference on Computer Vision and Pattern Recognition*, pages 4322–4330, 2019. 5

[44] Anian Ruoss, Maximilian Baader, Mislav Balunovic, and Martin T. Vechev. Efficient certification of spatial robustness. In *AAAI*, pages 2504–2513. AAAI Press, 2021. 1

[45] Anindya Sarkar, Anirban Sarkar, and Vineeth N. Balasubramanian. Enhanced regularizers for attributional robustness. In *AAAI*, pages 2532–2540. AAAI Press, 2021. 1

[46] Feng Shi, Jun Wang, Jun Shi, Ziyan Wu, Qian Wang, Zhenyu Tang, Kelei He, Yinghuan Shi, and Dinggang Shen. Review of artificial intelligence techniques in imaging data acquisition, segmentation and diagnosis for covid-19. *IEEE reviews in biomedical engineering*, 2020. 1, 6

[47] Amber L Simpson, Michela Antonelli, Spyridon Bakas, Michel Bilello, Keyvan Farahani, Bram Van Ginneken, Annette Kopp-Schneider, Bennett A Landman, Geert Litjens, Bjoern Menze, et al. A large annotated medical image dataset for the development and evaluation of segmentation algorithms, 2019. 7

[48] Eduardo Soares, Plamen Angelov, Sarah Biaso, Michele Higa Froes, and Daniel Kanda Abe. Sars-cov-2 ct-scan dataset: A large dataset of real patients ct scans for sars-cov-2 identification. *medRxiv*, 2020. 1, 6

[49] Christian Szegedy, Wojciech Zaremba, Ilya Sutskever, Joan Bruna, Dumitru Erhan, Ian Goodfellow, and Rob Fergus. Intriguing properties of neural networks, 2013. 1

[50] Florian Tramer, Nicholas Carlini, Wieland Brendel, and Aleksander Madry. On adaptive attacks to adversarial example defenses. In *NeurIPS*, 2020. 2

[51] Jonathan Uesato, Brendan O’donoghue, Pushmeet Kohli, and Aaron Oord. Adversarial risk and the dangers of evaluating against weak attacks. In *ICML*, pages 5025–5034. PMLR, 2018. 2, 5

[52] M Visser, DMJ Müller, RJM van Duijn, M Smits, N Verburg, EJ Hendriks, RJA Nabuurs, JCJ Bot, RS Eijgelaar, M Witte, et al. Inter-rater agreement in glioma segmentations on longitudinal mri. *NeuroImage: Clinical*, 22:101727, 2019. 7

[53] Martin Visser, Jan Petr, Domenique MJ Müller, Roelant S Eijgelaar, Eef J Hendriks, Marnix Witte, Frederik Barkhof, Marcel van Herk, Henk JMM Mutsaerts, Hugo Vrenken, et al. Accurate mr image registration to anatomical reference space for diffuse glioma. *Frontiers in neuroscience*, 14:585, 2020. 7

[54] He Wang, Feixiang He, Zhexi Peng, Tianjia Shao, Yong-Liang Yang, Kun Zhou, and David Hogg. Understanding the robustness of skeleton-based action recognition under adversarial attack. In *Proceedings of the IEEE/CVF Conference on Computer Vision and Pattern Recognition*, pages 14656–14665, 2021. 1

[55] Huaxia Wang and Chun-Nam Yu. A direct approach to robust deep learning using adversarial networks. In *ICLR*, 2019. 2

[56] Xiaosen Wang and Kun He. Enhancing the transferability of adversarial attacks through variance tuning. In *Proceedings of the IEEE/CVF Conference on Computer Vision and Pattern Recognition*, pages 1924–1933, 2021. 1

[57] Yisen Wang, Difan Zou, Jinfeng Yi, James Bailey, Xingjun Ma, and Quanquan Gu. Improving adversarial robustness requires revisiting misclassified examples. In *ICLR*, 2020. 2

[58] WHO. Coronavirus disease (covid-19) dashboard(<https://covid19.who.int/>). 2020. 1

[59] Tong Wu, Ziwei Liu, Qingqiu Huang, Yu Wang, and Dahua Lin. Adversarial robustness under long-tailed distribution.

In *Proceedings of the IEEE/CVF Conference on Computer Vision and Pattern Recognition*, pages 8659–8668, 2021. 1

- [60] Weibin Wu, Yuxin Su, Michael R Lyu, and Irwin King. Improving the transferability of adversarial samples with adversarial transformations. In *Proceedings of the IEEE/CVF Conference on Computer Vision and Pattern Recognition*, pages 9024–9033, 2021. 1
- [61] Yuxin Wu and Kaiming He. Group normalization. In *ECCV*, pages 3–19, 2018. 6
- [62] Han Xiao, Kashif Rasul, and Roland Vollgraf. Fashionmnist: a novel image dataset for benchmarking machine learning algorithms, 2017. 5
- [63] Shuo Yang, Tianyu Guo, Yunhe Wang, and Chang Xu. Adversarial robustness through disentangled representations. In *AAAI*, pages 3145–3153. AAAI Press, 2021. 1
- [64] Yunrui Yu, Xitong Gao, and Cheng-Zhong Xu. Lafat: Piercing through adversarial defenses with latent features. In *Proceedings of the IEEE/CVF Conference on Computer Vision and Pattern Recognition*, pages 5735–5745, 2021. 1
- [65] Hongyang Zhang, Yaodong Yu, Jiantao Jiao, Eric Xing, Laurent El Ghaoui, and Michael Jordan. Theoretically principled trade-off between robustness and accuracy. In *ICML*, pages 7472–7482. PMLR, 2019. 5
- [66] Jingfeng Zhang, Xilie Xu, Bo Han, Gang Niu, Lizhen Cui, Masashi Sugiyama, and Mohan Kankanhalli. Attacks which do not kill training make adversarial learning stronger. In *ICML*, pages 11278–11287. PMLR, 2020. 5
- [67] Jingfeng Zhang, Jianing Zhu, Gang Niu, Bo Han, Masashi Sugiyama, and Mohan Kankanhalli. Geometry-aware instance-reweighted adversarial training. In *ICLR*, 2021. 5